

RESOLVED SHOCK STRUCTURE OF THE BALMER-DOMINATED FILAMENTS IN TYCHO'S SUPERNOVA REMNANT : COSMIC RAY PRECURSOR?

JAE-JOON LEE,^{1,2} JOHN C. RAYMOND³, SANGWOOK PARK¹, WILLIAM P. BLAIR⁴, PARVIZ GHAVAMIAN⁵, P. F. WINKLER⁶,
 KELLY KORRECK³,

Draft version June 6, 2018

ABSTRACT

We report on the results from H α imaging observations of the eastern limb of Tycho's supernova remnant (SN1572) using the Wide Field Planetary Camera-2 on the Hubble Space Telescope. We resolve the detailed structure of the fast, collisionless shock wave into a delicate structure of nearly edge-on filaments. We find a gradual increase of H α intensity just ahead of the shock front, which we interpret as emission from the thin ($\sim 1''$) shock precursor. We find that a significant amount of the H α emission comes from the precursor and that this could affect the amount of temperature equilibration derived from the observed flux ratio of the broad and narrow H α components. The observed H α emission profiles are fit using simple precursor models, and we discuss the relevant parameters. We suggest that the precursor is likely due to cosmic rays and discuss the efficiency of cosmic ray acceleration at this position.

Subject headings: ISM: individual objects (G120.1+1.4) — ISM: supernova remnants — shock waves

1. INTRODUCTION

The shock transition in fast astrophysical shocks is intrinsically a “collisionless” process, and energy is dissipated via plasma turbulence and/or electromagnetic fields. An important consequence of the collisionless nature of the shocks is cosmic ray acceleration (e.g., Blandford & Eichler 1987). While there is increasing evidence of cosmic ray acceleration in supernova remnants, the details of the process are still not well understood, and the question of whether supernova remnants (SNRs) are the primary acceleration sites of Galactic cosmic rays is still open (Butt 2009).

Cosmic ray acceleration models require a precursor in which accelerated particles can scatter back to the postshock region for further acceleration. Observations of the cosmic ray precursor can constrain the two key parameters of acceleration models; the diffusion coefficient and the injection efficiency (Blandford & Eichler 1987; Boulares & Cox 1988). The Balmer-dominated filaments that are produced when fast SNR shocks propagate into partially neutral gas are potential sites where such a cosmic ray precursors can be observed. Most of the Balmer emission comes from a very narrow zone behind the shock, where the hydrogen atoms swept up by the shock are excited before they are ionized (Chevalier & Raymond 1978; Chevalier et al. 1980). However, in the presence of the precursor, additional Balmer emission is expected from the precursor region where the preshock gas is compressed and heated. Using

long-slit H α spectroscopy along the shock normal of a Balmer filament in Tycho's SNR, Lee et al. (2007, Lee07 hereafter) found that there is an increase of the H α narrow component intensity in a small region ($\sim 0.4''$) ahead of the shock front, which they proposed as potential emission from the precursor. However, the angular resolution of the observation by Lee07 is $\sim 0.5''$ and their results needed to be verified with high resolution observations.

In this *Letter*, we report H α imaging observations of Balmer-dominated filaments in Tycho's SNR using the Wide Field and Planetary Camera 2 (WFPC2) on the Hubble Space Telescope (HST), which resolves the detailed structure of the shock. § 2 presents the observations and reports the detection of the precursor. The precursor is modeled in § 3 and its characteristics are discussed in § 4. Finally in § 5, we discuss the efficiency of cosmic ray acceleration in this region.

2. OBSERVATIONS AND RESULTS

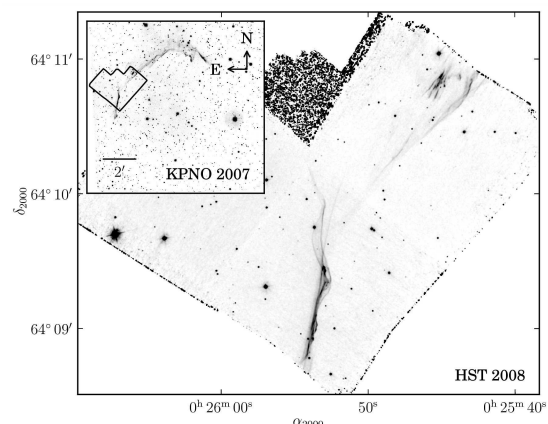


FIG. 1.— Hubble Space Telescope image of the Balmer-dominated filaments in the northeastern part of Tycho's SNR. The WFPC2 detector with F656N filter was used. The inset shows an H α image toward Tycho's SNR from a ground-based telescope (KPNO). The area observed by HST is marked.

¹ Astronomy and Astrophysics Department, Pennsylvania State University, University Park, PA 16802, USA

² lee@astro.psu.edu

³ Harvard-Smithsonian Center for Astrophysics, 60 Garden Street, Cambridge, MA 02138, USA

⁴ Department of Physics and Astronomy, Johns Hopkins University, 3400 N. Charles St., Baltimore, MD 21218, USA

⁵ Space Telescope Science Institute, 3700 San Martin Drive, Baltimore, MD, 21218, USA

⁶ Department of Physics, Middlebury College, Middlebury, VT 05753, USA

We observed the eastern limb of Tycho’s SNR using WFPC2 on HST. The observations were conducted on Mar 23, 2008, with the camera arranged to cover knot g, one of the brightest H α filaments in the remnant ($\alpha_{2000}, \delta_{2000}=00^{\text{h}} 25^{\text{m}} 52^{\text{s}}, +64^{\circ} 09' 21''$). A total of 10 exposures, each with 2600 \sim 2700 sec, were obtained using the F656N H α filter, which has a central wavelength of 6564Å. The filter has a bandwidth of 54 Å ($\sim 2500 \text{ km s}^{-1}$), which is comparable to the velocity width of the H α broad component in this region (Ghavamian et al. 2001), and transmits about half of the broad component flux. Images are combined and “drizzled” onto a $0.06'' \text{ pixel}^{-1}$ scale using the IRAF task *multidrizzle* (Fruchter & Hook 2002), which also detects and removes cosmic-rays. The PSF of the final drizzled image has a FWHM of $\sim 0.18''$.

The full field observed with HST is shown in Fig. 1. The brightest filaments, comprising the knot g region and associated filaments, are seen on the WF3 chip, while fainter filaments belonging to the northeastern limb of the SNR are visible on the WF4 chip. The superb angular resolution of HST reveals details of the filaments not available from ground-based telescopes. This is more clearly seen in Fig. 2, where we compare the close-up view of the knot g region to the image observed with a ground-based telescope (CCD image obtained at the KPNO 2.1m telescope on 2007 October 4) at the same scale. The HST image reveals a faint extension of the emission toward upstream (to the east) along most of the bright part of the filaments (between $\delta=64^{\circ} 08' 40''$ and $\delta=64^{\circ} 09' 20''$). This extension is more clearly demonstrated by the H α brightness profiles from the cuts along the shock normals, as seen in Fig. 3. The profiles show a bright emission peak of thickness $\lesssim 0.5''$, which is the emission from neutral hydrogen excited in the postshock area. The small bumps around offsets $-1.8''$ and $0.7''$ are likely due to the projection of fainter tangencies of the rippled shock front to the line of sight. The H α emission slowly falls off not only toward the downstream but also toward the upstream direction. In the downstream, the H α emission is emitted within a very narrow region behind the shock as neutral hydrogen is rapidly ionized. Thus, we consider that the downstream emission is likely a projection of the curved shock fronts. Some of the upstream emission could be in principle attributed to a similar projection effect. However, Fig. 2 shows that the shock front in this region does not show any significant curvature, and it is difficult to devise a shock geometry that explains both upstream and downstream emission. Fig. 4 shows emission profiles along different cuts, and the upstream emission components are similarly seen. The upstream emission is also seen faintly in the profile of cut 01 where the shock surface is apparently convex (see Fig. 2), and a projection effect is not likely to explain the upstream emission. Therefore, we propose that the faint emission from the upstream region represents the emission mostly from the neutral hydrogen atoms excited in a shock precursor, and the effect of shock geometry makes only a minor contribution.

3. MODELING THE PRECURSOR EMISSION

To estimate the physical properties of the precursor, we model the observed spatial H α emission profiles (Fig. 4). We first try a simple toy precursor model. We assume

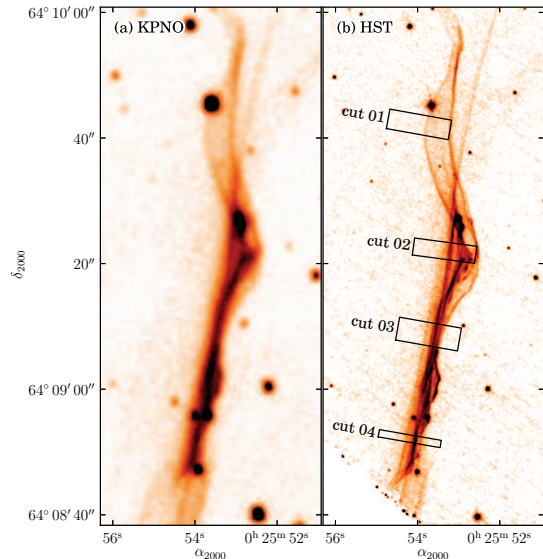


FIG. 2.— (a) The H α image of knot g, one of the brightest Balmer-dominated filaments in Tycho, taken by KPNO 2.1m telescope. (b) The HST image of the same region. The black rectangles are regions from which the brightness profiles are extracted.

a shock front located at $x = x_0$ with increasing x toward downstream. The H α emission from the postshock region is assumed to be confined to a region of thickness of w with a uniform emissivity. In the precursor, the H α emissivity peaks at the shock front and decreases exponentially away from the shock front. The profile is written as

$$y = \begin{cases} 0 & \text{if } x - x_0 > w \\ Fw^{-1} & \text{if } 0 \leq x - x_0 \leq w \\ FfL^{-1}e^{(x-x_0)/L} & \text{if } x - x_0 < 0 \end{cases}$$

where F is the total H α flux from the postshock region, L is the precursor length scale, and f is a flux ratio of the precursor to the postshock region. The variation in the downstream region could be modeled with a curved geometry of the shock. However, we find that the observed variation cannot be adequately fit by shocks of a simple geometry. Instead of introducing arbitrary fit parameters to describe the structure along the line of sight, we simply assume plane-parallel shocks and ignore the data where the model deviates from the observation. As long as L is sufficiently smaller than the local curvature radii of the shocks, the plane-parallel assumption will not significantly affect estimated precursor parameters. As evident from Fig. 2, the profiles require multiple shock components projected along the line of sight. To minimize the number of free parameters, we assume that shocks have the same profile shape, i.e., parameters f , L and w are tied among multiple shocks for a given profile cut from Fig. 2. The model profiles are Gaussian smoothed to account for the instrumental profile.

The fits are shown in Fig. 4, and the results are summarized in Table 1. We find that the H α flux from the precursor region is comparable to that of the postshock area ($f \sim 1$), with L around $1''$, corresponding to $3 \times 10^{16} \text{ cm}$ at the assumed distance of 2.1 kpc to Tycho (Kamper & van den Bergh 1978; Ghavamian et al. 2001). The thicknesses of the postshock emitting area are around $\sim 0.3''$. A relatively large L of $\sim 2''$ is found

TABLE 1
FIT PARAMETERS FROM THE TOY PRECURSOR MODEL

	f	L ["]	w ["]	$\chi^2/\text{d.o.f.}$
cut 01	$1.4^{+0.3}_{-0.2}$	$2.5^{+0.7}_{-0.5}$	$0.42^{+0.06}_{-0.05}$	206/170
cut 02	$0.72^{+0.06}_{-0.06}$	$1.2^{+0.1}_{-0.1}$	$0.31^{+0.02}_{-0.02}$	170/182
cut 03	$0.57^{+0.04}_{-0.03}$	$0.70^{+0.06}_{-0.05}$	$0.35^{+0.01}_{-0.01}$	258/182
cut 04	$0.93^{+0.04}_{-0.03}$	$0.87^{+0.05}_{-0.05}$	$0.39^{+0.02}_{-0.02}$	220/182

in cut 01, but this is likely to be overestimated due to the much stronger local curvature of the shock in this region. We also note that, for profiles in cuts 02 and 03, where the structure of the overlapping shocks is quite complex, the fitted precursor parameters are somewhat sensitive to the assumed baseline and also the number of shock components. These can cause $\sim 20 - 30\%$ systematic uncertainties on the fitted parameters.

We now consider a more realistic precursor model that assumes an exponential temperature profile (similar to the above toy model) in the precursor. The model calculates the ionization of hydrogen atoms throughout the shock and the emissivity of $\text{H}\alpha$ and $\text{Ly}\beta$ lines. The radiative transfer of the $\text{Ly}\beta$ line is computed using the Monte Carlo technique to account for the $\text{H}\alpha$ enhancement by $\text{Ly}\beta$ -trapping. The model has been utilized by Wagner et al. (2009) to interpret the result of Lee07. We adopt the parameters used in Wagner et al. (2009); shock velocity of 2000 km s^{-1} , preshock density of 1 cm^{-3} , and the preshock neutral fraction of 0.85. More details of the model and the input parameters can be found in Wagner et al. (2009). The extensive discussion of the detailed modeling and associated uncertainties is beyond the scope of this *Letter*, and here we simply present a brief summary of the results. For cuts 02, 03, and 04, we estimate peak temperatures in the precursor $T_{\text{peak}} = 80,000 \sim 100,000 \text{ K}$, and the precursor length scale $L = 5 \sim 7 \times 10^{16} \text{ cm}$. As in the toy model, a larger length scale is required for cut 01. The estimated length scales of the precursor are generally larger than those estimated from the simple toy model. This is because the $\text{H}\alpha$ emissivity is sensitive to the temperature, i.e., the emissivity profile increases more rapidly than the temperature profile, thus effectively reducing the length scale. We note that the precursor parameters are in agreement with the results of Wagner et al. (2009), while the length scale is slightly larger.

4. ORIGIN OF THE PRECURSOR

The existence of a thin precursor has been suggested from previous observations. The spectral profiles of the $\text{H}\alpha$ narrow component traces the velocity distribution of the gas entering the shocks, and those observed in SNRs have widths of $40 - 60 \text{ km s}^{-1}$ (e.g., Smith et al. 1994; Sollerman et al. 2003). This is too large for the temperature of the ambient gas, as all the hydrogen would have been ionized at the implied temperature and no Balmer filament should exist. Instead, the observed line width is suggested to represent the gas heated in the precursor, which is thin enough for the preshock neutrals not to be completely ionized. Also, the observed flux ratio of the $\text{H}\alpha$ broad component and the narrow component was sometimes found to be smaller than what models predict (e.g., Ghavamian et al. 2003; Rakowski et al. 2009),

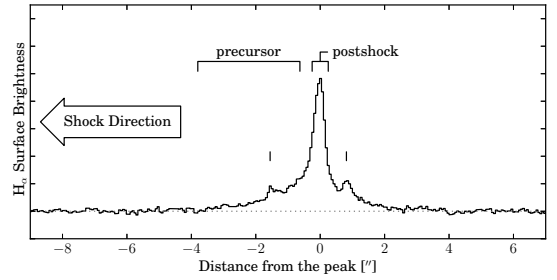


FIG. 3.— $\text{H}\alpha$ brightness profile across the shock normal extracted from cut 04. The bright narrow peak is believed to correspond to the emission from the narrow region of the immediate postshock area. The emission extends up to $4''$ toward upstream, which is interpreted as emission from the shock precursor. The small bumps in the profile (marked with small vertical bars) are likely the projection of other shock fronts.

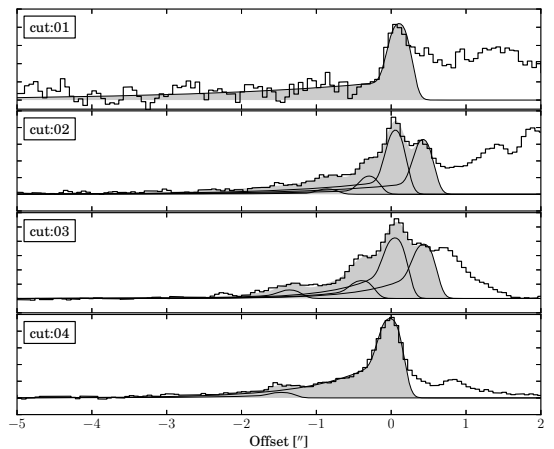


FIG. 4.— $\text{H}\alpha$ brightness profiles across the shock normals in different regions marked in Fig. 2. The profiles are fitted with multiple components of toy precursor models. The gray area represents the accumulated emission from all models, and the solid lines represent emission from projected individual shocks.

and the excessive narrow component emission was attributed to the contribution of emission from the precursor (Ghavamian et al. 2001; Rakowski et al. 2009).

The characteristics of the precursor revealed by our HST observations are consistent with results from previous observations. The peak temperature in the precursor may be relatively higher than the temperature implied by the line width of the $\text{H}\alpha$ narrow component. However, the temperature we modeled is the electron temperature, which might not be in equilibrium with the neutral hydrogen atoms. Also, the velocity profiles of the $\text{H}\alpha$ emission could deviate from a Gaussian profile (Ghavamian et al. 2001; Lee et al. 2007; Raymond et al. 2010), and a simple line width may not be an adequate temperature indicator. Our observations show that the emission from the precursor is a significant contributor to the $\text{H}\alpha$ narrow component. We estimate that the precursor emission may contribute up to 30-40% of the narrow component for a slit width of $1''$. The narrow component emission from the precursor will affect estimates of electron-ion equilibration based on the observed broad-to-narrow intensity ratio (Ghavamian et al. 2001; Heng & McCray 2007; Rakowski et al. 2009). For those SNRs where the observed $\text{H}\alpha$ broad-to-narrow flux ratio was smaller than the model predictions, accounting for

the precursor could bring them into agreement.

The likely candidates for producing this precursor are a cosmic ray precursor or a fast neutral precursor (Smith et al. 1994; Hester et al. 1994). While our HST results provide detailed structure of the precursor, models of these precursors are not available for a quantitative comparison. However, the cosmic ray precursor scenario has been preferred over the fast neutral precursor for various reasons (see Lee07 and references therein). Also, the growing evidence of cosmic ray acceleration in Tycho's SNR supports the existence of cosmic ray precursor (e.g., Warren et al. 2005).

Wagner et al. (2009) computed a series of time dependent numerical simulations of cosmic ray modified shocks, tuning the model parameters to reproduce the precursor characteristics of Lee07. The results of Wagner et al. (2009) can be a plausible approximation as the estimated precursor properties are not much different. They found that, assuming a distance of 2.1 kpc to Tycho's SNR, the CR diffusion coefficient, κ , the injection parameter, ϵ , and the timescale for the energy transfer, τ , of $\kappa = 2 \times 10^{24} \text{ cm}^2 \text{ s}^{-1}$, $\epsilon = 4.2 \times 10^{-3}$, and $\tau = 426 \text{ yr}$ is required to describe the observations. The length scales of the precursor estimated from our new observation are slightly larger than that of Lee07. The larger precursor length scale requires a larger cosmic ray diffusion coefficient. This increases the acceleration time scale, so the cosmic ray injection parameter may need to be increased to compensate for the slower acceleration. While some fine tuning of the parameters may be required, we believe that Wagner et al.'s findings, e.g., that the cosmic ray acceleration is not very efficient in this shock and about 10% of the shock energy has converted to cosmic rays, are still valid.

5. COSMIC RAY ION ACCELERATION IN TYCHO

The existence of the cosmic ray precursor does not necessarily imply efficient cosmic ray acceleration. For the Balmer-dominated filaments to be observable, some neutral hydrogen needs to survive ionization in the precursor. As efficient cosmic ray acceleration tends to make the precursor wider and hotter, the Balmer-dominated filaments may not trace the shocks having efficient cosmic ray acceleration (cf. Helder et al. 2009). For the shock studied in this paper, a more direct suggestion of inefficient acceleration can be inferred from the results of Lee07. From the difference in radial velocity of the preshock gas and the H α narrow component emitted in the postshock region, they estimated the amount of gas deceleration in the precursor. The preshock gas is decelerated in the precursor due to the gradient of the cosmic

ray pressure by about a few hundred km s^{-1} based on the radial velocity measurements. The value is not sensitive to the assumed distance, and is significantly smaller than the measured line width of the broad component. In this shock, the thermal pressure of the ordinary gas still dominates over the cosmic ray pressure and the acceleration is not likely to be very efficient.

Throughout the discussion, we have assumed that the distance to Tycho's SNR is 2.1 kpc. The measurement is based on the estimated proton temperature (from the observed line width of the broad component) and the optical proper motion, assuming no cosmic ray acceleration at the shock. The cosmic ray acceleration, if significant, can effectively reduce the postshock temperature (see Helder et al. 2009, and references therein); thus the distance may have been underestimated. However, as has been discussed above, the optical observations are consistent with cosmic ray acceleration not being very efficient in this region, so the distance of 2.1 kpc, derived assuming no cosmic ray acceleration, remains a reasonable value.

Using Chandra observations, Warren et al. (2005) found the locations of the shock front (SF) and the contact discontinuity (CD) along the boundary of the remnant. They interpreted the small separation between the two as an indication of efficient cosmic ray acceleration. The region of knot g is one of the regions where the SF-CD separation is smallest (except those regions of ejecta protrusion). A simple extrapolation of their argument will lead to the most efficient cosmic ray acceleration in this region, being inconsistent with our results. However, the region around knot g is where the remnant could be interacting with dense ambient clouds (Reynoso et al. 1997; Lee et al. 2004). Thus, the small SF-CD separation in this region could be due to a recent encounter of the shock with the dense ambient gas, instead of efficient cosmic ray acceleration.

In conclusion, we have presented high resolution H α imaging observations of Tycho, revealing the existence of a thin precursor which we interpret as a cosmic ray precursor. While the current observation is consistent with inefficient acceleration, the observation of the precursor itself provides an important opportunity to constrain the key parameters of the acceleration, such as the diffusion coefficient and the injection parameters. A comparison with detailed numerical simulations will be critical to study the detailed physics of cosmic ray acceleration.

This research was supported by STScI grant GO-11184.01-A-R to the Smithsonian Astrophysical Observatory.

Facilities: HST (WFPC2), KPNO2m

REFERENCES

- Blandford, R., & Eichler, D. 1987, *Phys. Rep.*, 154, 1
 Boulares, A., & Cox, D. P. 1988, *ApJ*, 333, 198
 Butt, Y. 2009, *Nature*, 460, 701
 Chevalier, R. A., Kirshner, R. P., & Raymond, J. C. 1980, *ApJ*, 235, 186
 Chevalier, R. A., & Raymond, J. C. 1978, *ApJ*, 225, L27
 Fruchter, A. S., & Hook, R. N. 2002, *PASP*, 114, 144
 Ghavamian, P., Rakowski, C. E., Hughes, J. P., & Williams, T. B. 2003, *ApJ*, 590, 833
 Ghavamian, P., Raymond, J., Smith, R. C., & Hartigan, P. 2001, *ApJ*, 547, 995
 Helder, E. A., Vink, J., Bassa, C. G., Bamba, A., Bleeker, J. A. M., Funk, S., Ghavamian, P., van der Heyden, K. J., Verbunt, F., & Yamazaki, R. 2009, *Science*, 325, 719
 Heng, K., & McCray, R. 2007, *ApJ*, 654, 923
 Hester, J. J., Raymond, J. C., & Blair, W. P. 1994, *ApJ*, 420, 721
 Kamper, K. W., & van den Bergh, S. 1978, *ApJ*, 224, 851
 Lee, J., Koo, B., Raymond, J., Ghavamian, P., Pyo, T., Tajitsu, A., & Hayashi, M. 2007, *ApJ*, 659, L133
 Lee, J., Koo, B., & Tatematsu, K. 2004, *ApJ*, 605, L113
 Rakowski, C. E., Ghavamian, P., & Laming, J. M. 2009, *ApJ*, 696, 2195

- Raymond, J. C., Frank, P. F., Blair, W. P., Lee, J., & Park, S. W. 2010, *ApJ*, submitted
- Reynoso, E. M., Moffett, D. A., Goss, W. M., Dubner, G. M., Dickel, J. R., Reynolds, S. P., & Giacani, E. B. 1997, *ApJ*, 491, 816
- Smith, R. C., Raymond, J. C., & Laming, J. M. 1994, *ApJ*, 420, 286
- Sollerman, J., Ghavamian, P., Lundqvist, P., & Smith, R. C. 2003, *A&A*, 407, 249
- Wagner, A. Y., Lee, J., Raymond, J. C., Hartquist, T. W., & Falle, S. A. E. G. 2009, *ApJ*, 690, 1412
- Warren, J. S., Hughes, J. P., Badenes, C., Ghavamian, P., McKee, C. F., Moffett, D., Plucinsky, P. P., Rakowski, C., Reynoso, E., & Slane, P. 2005, *ApJ*, 634, 376